



Article

Selective Catalytic Reduction of NO with H₂ over Pt/Pd-Containing Catalysts on Silica-Based Supports

Magdalena Jabłońska ^{1,*}, Adrián Osorio Hernández ¹, Jürgen Dornseiffer ², Jacek Grams ³, Anqi Guo ⁴, Ulrich Simon ⁴ and Roger Gläser ¹

- ¹ Institute of Chemical Technology, Universität Leipzig, Linnéstr. 3, 04103 Leipzig, Germany; adrian.osorio@uni-leipzig.de (A.O.H.)
- Institute of Energy Materials and Devices, Materials Synthesis and Processing (IMD-2), Forschungszentrum Jülich GmbH, 52425 Jülich, Germany; j.dornseiffer@fz-juelich.de
- ³ Institute of General and Ecological Chemistry, Faculty of Chemistry, Lodz University of Technology, Zeromskiego 116, 90-924, Lodz, Poland
- Institute of Inorganic Chemistry, RWTH Aachen University, Landoltweg 1a, 52074 Aachen, Germany
- * Correspondence: magdalena.jablonska@uni-leipzig.de

Abstract: Platinum- and/or palladium-containing silica-based supports were applied for the selective catalytic reduction of NO_x with hydrogen (H₂-SCR-DeNO_x). To obtain enhanced activity and N₂ selectivity below 150 °C, we varied the type and loading of noble metals (Pt and Pd both individually and paired, 0.1–1.0 wt.-%), silica-containing supports (ZrO₂/SiO₂, ZrO₂/SiO₂/Al₂O₃, Al₂O₃/SiO₂/TiO₂), as well as the H₂ concentration in the feed (2000–4000 ppm). All of these contributed to enhancing N₂ selectivity during H₂-SCR-DeNO_x over the (0.5 wt.-%)Pt/Pd/ZrO₂/SiO₂ catalyst in the presence of 10 vol.-% of O₂. H₂ was completely consumed at 150 °C. A comparison of the catalytic results obtained during H₂-SCR-DeNO_x, (H₂-)NH₃-SCR-DeNO_x, as well as stop-flow H₂-SCR-DeNO_x and temperature-programmed studies, revealed that in the temperature range between 150 and 250 °C, the continuously coupled or overlaying mechanism of NO reduction by hydrogen and ammonia based on NH₃ formation at lower temperatures, which is temporarily stored at the acid sites of the support and desorbed in this temperature range, could be postulated.

Keywords: noble metals; Pt–Pd; hydrogen; H₂-SCR-DeNO_x; reaction mechanism

Academic Editors: Mario J. Muñoz-Batista and Akira Otsuki

Received: 17 April 2025 Revised: 12 May 2025 Accepted: 14 May 2025 Published: 15 May 2025

Citation: Jabłońska, M.; Osorio Hernández, A.; Dornseiffer, J.; Grams, J.; Guo, A.; Simon, U.; Gläser, R. Selective Catalytic Reduction of NO with H2 over Pt/Pd-Containing Catalysts on Silica-Based Supports. *Catalysts* 2025, 15, 483. https://doi.org/10.3390/ catal15050483

Copyright: © 2025 by the authors. Licensee MDPI, Basel, Switzerland. This article is an open access article distributed under the terms and conditions of the Creative Commons Attribution (CC BY) license (https://creativecommons.org/licenses/by/4.0/).

1. Introduction

Emissions of nitrogen oxides (NO_x: NO and NO₂) from stationary and mobile sources affect human health and the environment (e.g., [1,2]). The selective catalytic reduction of NO_x with hydrogen (H₂-SCR-DeNO_x) with an efficiency of up to 90% is applicable in various sectors, including power generation and transport [3–5]. This innovative process replaces NH₃-SCR-DeNO_x, particularly in industrial power stations using hydrogen, such as H₂ engines for combined heat and power (CHP) with exhaust gas temperatures below 150 °C. The extensive investigation of materials specifically tailored for H₂-SCR-DeNO_x is still ongoing as many catalysts promote severe N₂O formation in the low-temperature range (below 200 °C). Different supports (e.g., SiO₂, Al₂O₃, ZrO₂, mesoporous silicas, zeolites ZSM-5, or SSZ-13 [6–9]) vary the dispersion of the active components (such as Pt, Pd [10,11], including promotors W, Mo, Cr [12–14], etc.) and thus the activity and N₂ selectivity of the final catalyst as well as the reaction pathways. Properties such as the

Catalysts 2025, 15, 483 2 of 16

redox and acidity of the support, together with its interactions with noble metals, are frequently reported as the determinants of the catalytic properties in H₂-SCR-DeNO_x (e.g., [15,16]). For example, Shibata et al. [16] reported the relationship between the integrated white line intensity of the Pt Liii-edge XANES spectrum and the turnover frequency for NO_x (TOF), estimated from the NO_x conversion and Pt dispersion. The oxidation state of Pt was assumed to be the controlling the H2-SCR-DeNOx activity, which decreased among the investigated catalysts as follows: $Pt/SiO_2 > Pt/SiO_2 - Al_2O_3 > Pt/ZSM-5$ (n(Si)/n(Al) = 20), Pt/MOR (mordenite, n(Si)/n(Al) = 7.7) > Pt/Al₂O₃ > Pt/MgO. The N₂ selectivity on Ptcontaining zeolites was higher than on oxide-supported Pt, which was related to the different amount of Brønsted acid sites (NH₄*) on the respective catalyst, as detected using FT-IR spectroscopy. Costa and Efstathiou [17] reported the correlation between Pt dispersion (estimated from H₂ chemisorption) and the specific rate of N₂ formation over Pt/MgO-CeO₂. A reduction in Pt dispersion from 90% (for 0.1 wt.-% Pt loading) to 10% (for 2 wt.-% Pt loading) led to a decrease in the specific integral rate of № formation by more than an order of magnitude. Yu et al. [18] reported that the valance states of Pt (80% in Pt 0 , 20% in Pt 2 O) in Pt-ZSM-35 (n(Si)/n(Al) = 15) remain independent from noble metal loading (0.5–2.0 wt.-%). They attributed the low activity in 2 wt.-% Pt/ZSM-35 to the blockage of the acid sites and the aggregation of Pt species (as confirmed by XRD and TEM analyses). Conversely, Park et al. [11] reported higher NO_x conversion for catalysts aged up to 850 °C, despite a reduction in the acid sites and Pt particle sintering. Thus, these results indicate the need for systematic studies on particular groups of H2-SCR-DeNO_x catalysts, as their activity and N₂ selectivity may vary depending on the applied catalyst preparation and treatment as well as the reaction conditions.

Additionally, Pt-containing catalysts and Pd-containing materials have been documented in this reaction due to their lower price and frequently higher N₂ selectivity than Pt-based catalysts. For example, Pd supported on inorganic oxides, such as TiO₂-Al₂O₃ or ZrO₂-CeO₂ (80–87% NO conversion at 150–180 °C) had more than 80% N₂ selectivity below 180 °C [19,20], and Pd-ZSM-5 was reported to possess more than 95% NO_x activity and N₂ selectivity at 150 °C [21]. Recently, we summarized the current status of the Pt-based (and partly Pd-based) catalysts in H₂-SCR-DeNO_x in a review article [22].

In this work, Pt and/or Pd supported on selected silica-based supports were evaluated in H₂-SCR-DeNO_x for their activity and N₂ selectivity in a feed containing 10 vol.-% O₂. Although numerous investigations refer to Pt- or Pd-containing catalysts separately, to the best of our knowledge, this is the first time that the performance of Pt-Pd-containing catalysts is reported. Furthermore, none of the studies reported so far compared Pt- and Pd-containing catalysts under the same reaction conditions. Systematic investigations of these catalysts will provide a fundamental basis for a knowledge-driven catalyst design and improvement for industrial application.

2. Results

Figures S1–S3 together with Tables S1 and S2 show the results of the physicochemical characterization of the selected samples. The powder XRD patterns of the ZrO₂/SiO₂-based samples mainly revealed Bragg reflexes characteristic of ZrO₂ (cubic) at 2 theta values of 30.2°, 35.0°, 50.4°, 60.2°, and 63.0° (e.g., [23,24]). Otherwise, the ZrO₂/SiO₂/Al₂O₃-based samples showed an amorphous phase. For the Al₂O₃/SiO₂/TiO₂-based samples, the reflexes mainly occurred at 2 theta of 25.3°, 37.8°, 48.0°, 54.0°, 55.2°, and 62.7°, indicating TiO₂ (anatase) as the main crystalline phase of these materials (e.g., [25]). Thus, our XRD analysis revealed that the alumina-silica-based support interspersed with TiO₂ particles. The N₂ sorption analysis showed that the analyzed samples possessed mesopores up to 30 nm. The elemental analysis revealed a slightly higher amount of Pt (0.73–0.77 wt.-%) than the intended amount. Furthermore, in the Pt–Pd-containing

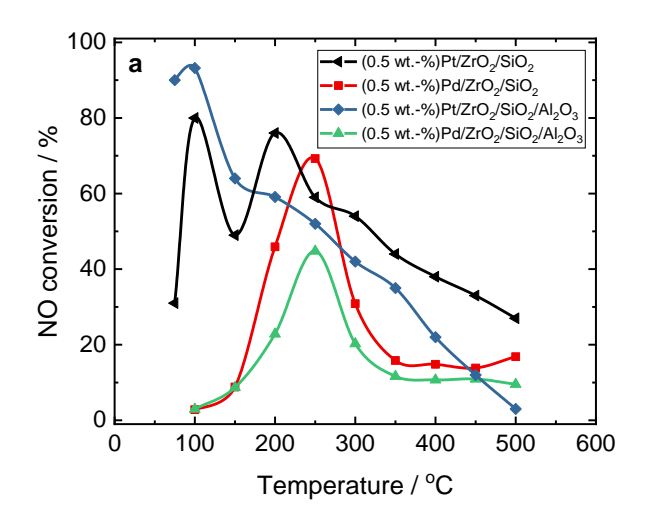
Catalysts 2025, 15, 483 3 of 16

samples, nearly two times the amount of Pt was compared with the Pd species (Table S1). Figure S3 shows the NH₃-TPD profiles for the investigated materials. For comparative purposes, an NH₃-TPD study was also performed over Pt-, Pd-, and Pt-Pd-containing catalysts, showing no significant effect of the precious metal component on the NH₃-TPD profile. Similar findings were obtained previously over Mo/ZrO₂ and Pt-doped Mo/ZrO₂ [26]. As can be seen, NH₃ desorbed mainly in one broad peak up to 350 °C, with a broad shoulder for Al-containing samples above 350 °C. Based on the NH₃-TPD analysis (Figure S3, Table S3), the Al-containing materials possessed the highest concentration of acid sites, up to 343 μmol g⁻¹, for titania containing Pt/Pd/Al₂O₃/SiO₂/TiO₂ (30/10) catalyst. However, taking into account the specific surface area of the samples (Table S2), Pt/ZrO₂/SiO₂ had a higher acid site density than Pt/ZrO₂/SiO₂/Al₂O₃ (1.47 versus 1.22 μmol m⁻²). Due to the relatively low Pt and Pd loading, we could not determine the valance state of catalysts. However, Li et al. [27] asserted that Pt appears as Pt²⁺O in Pt/ZrO₂ (calcined at 500 °C in air for 10 h) [28].

2.1. Results of Catalytic Studies

2.1.1. Type of Precious Metal

Figure 1 compares the activity and N₂ selectivity of Pt- or Pd-containing ZrO₂/SiO₂ and ZrO₂/SiO₂/Al₂O₃ in H₂-SCR-DeNO_x. The NO conversion as a function of temperature shows a *volcano*-shaped profile for all catalysts, although less pronounced in the case of Pd-containing catalysts. The NO reduction over Pt-containing catalysts enhanced between 75–100 °C compared to those containing Pd species (150–350 °C). Furthermore, Pt-based ZrO₂/SiO₂/Al₂O₃ had slightly higher activity and N₂ selectivity than Pt/ZrO₂/SiO₂. The NO reduction behavior at a maximum at 100 °C over the Pt-based catalysts (especially for Pt/ZrO₂/SiO₂) arose due to the NO reduction with H₂ according to Equation (1) (e.g., [5,29,30]). The observed high amount of nitrous oxide in this temperature range is caused by the dissociative adsorption of NO on the active precious metal sites, followed by a rearrangement of the adsorbed species and desorption of N₂O and H₂O via Equations (2)–(4).



Catalysts 2025, 15, 483 4 of 16

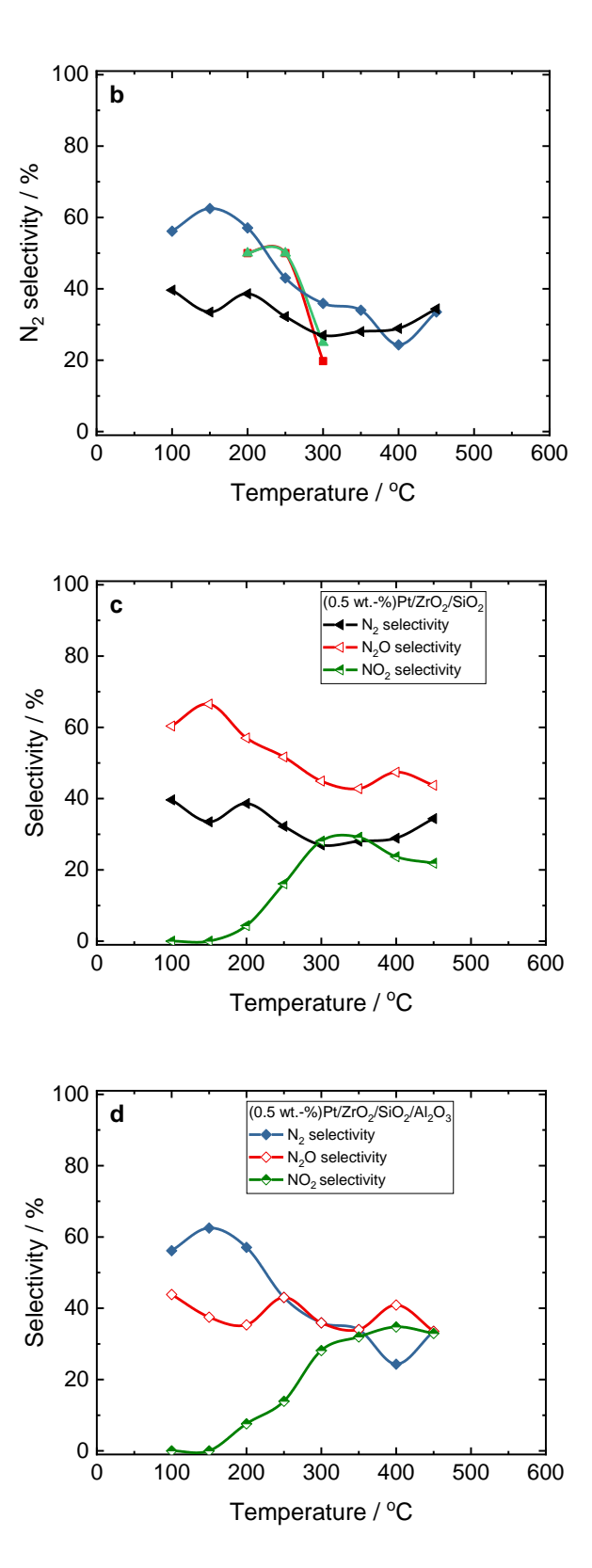


Figure 1. (a) NO conversion and (b–d) selectivity over Pt- and Pd-containing ZrO₂/SiO₂ and ZrO₂/SiO₂/Al₂O₃ catalysts during H₂-SCR-DeNO_x; (a,b) sample labels are equal; reaction conditions: $m_K = 0.1$ g, c(NO) = 200 ppm, $c(H_2) = 2000$ ppm, $c(O_2) = 10$ vol.-%, diluted in He, F_{TOT} = 200 mL min⁻¹, GHSV = 30,000 h⁻¹.

$$2 \text{ NO} + 2 \text{ H}_2 \rightarrow \text{ N}_2 + 2 \text{ H}_2\text{O}$$
 (1)

$$2 \text{ NO} \rightarrow 2 \text{ N}_{ads} + 2 \text{ O}_{ads} \rightarrow \text{ N}_2\text{O} + \text{O}_{ads}$$
 (2)

Catalysts 2025, 15, 483 5 of 16

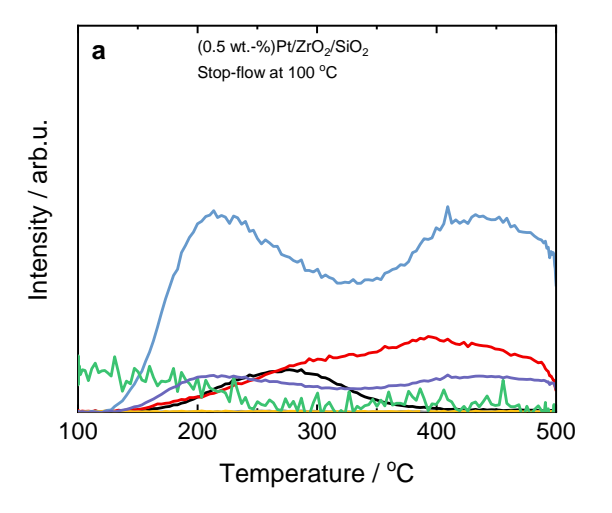
$$H_2 \rightarrow 2 H_{ads}$$
 (3)

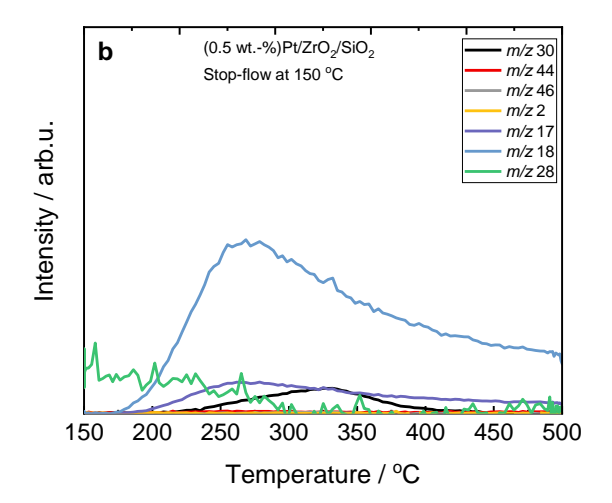
$$O_{ads} + 2 H_{ads} \rightarrow H_2O \tag{4}$$

As H₂ is completely consumed at 150 °C (Equation (5)), the *real* H₂-SCR-DeNO_x takes place only below this temperature (Figures S4 and S5).

$$2 H_2 + O_2 \rightarrow 2 H_2O$$
 (5)

At 150 °C, NO is preferentially adsorbed on the surface of ZrO₂/SiO₂-based catalysts as NO_{ads}, which dissociates into N_{ads} and O_{ads} species with the formation of N₂O (Equation (2)). To prove the adsorption of NO on the surface of ZrO₂/SiO₂-based catalysts at this temperature, we performed stop-flow experiments. H₂-SCR-DeNO_x was performed for 45 min (simulating a single step of the process); after that, the feed was exchanged for pure helium for 90 min. Finally, the temperature was increased up to 500 °C. The results revealed an accumulation of NO on the surface of the ZrO₂/SiO₂-based catalysts (Figures 2 and S6). Interestingly, the NO conversion curve for Pt/ZrO₂/SiO₂ shows a second maximum at 200 °C, which suggests a second reaction pathway.





Catalysts 2025, 15, 483 6 of 16

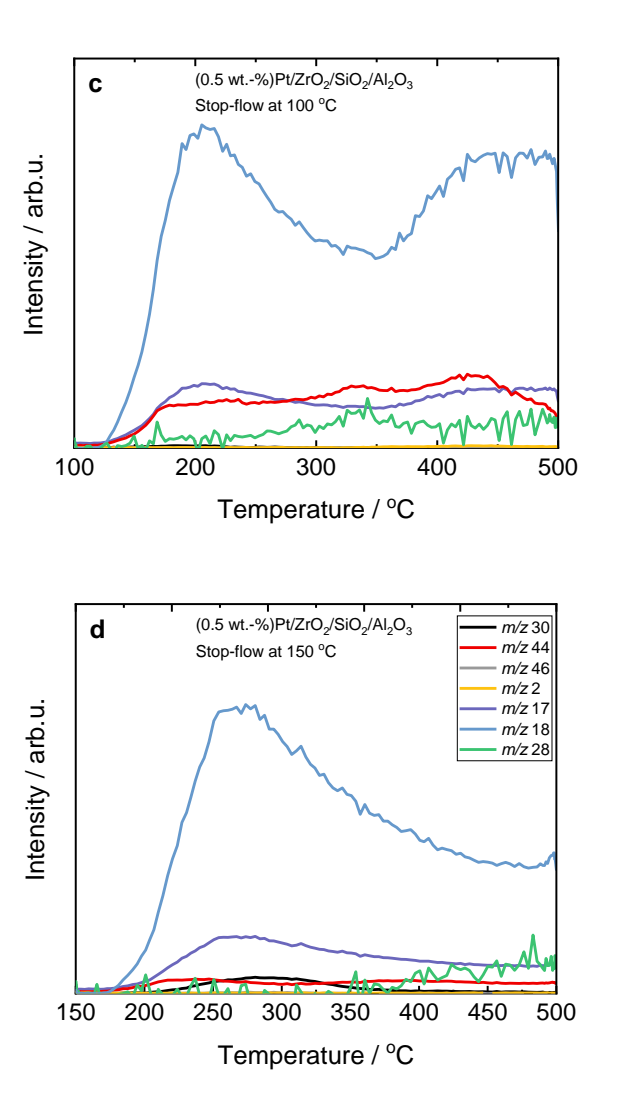


Figure 2. Stop-flow H₂-SCR-DeNO_x experiments over (**a**,**b**) Pt-containing ZrO₂/SiO₂ and (**c**,**d**) ZrO₂/SiO₂/Al₂O₃ catalysts; (**a**–**d**) labels are equal; reaction conditions: $m_K = 0.1$ g, c(NO) = 200 ppm, $c(H_2) = 2000$ ppm, $c(O_2) = 10$ vol.-%, diluted in He, F_{TOT} = 200 mL min⁻¹, GHSV = 30,000 h⁻¹ (m/z – mass-to-charge ratio). H₂ (m/z 2), N₂ (m/z 28), NO (m/z 30), N₂O (m/z 44), and NO₂ (m/z 46).

2.1.2. H2-SCR-DeNOx Versus NH3-SCR-DeNOx and H2-NH3-SCR-DeNOx

The catalytic properties of selected Pt-containing samples were evaluated in NH₃-SCR-DeNO_x, as shown in Figure S7. Cleary, Pt-based ZrO₂/SiO₂/Al₂O₃ reduced more NO with NH₃, while the selectivity of both materials remained nearly the same. In addition, the maximum NO conversion in NH₃-SCR-DeNO_x for Pt/ZrO₂/SiO₂ at 200 °C was in the same temperature range where the second peak in H₂-SCR-DeNO_x occurred (compared to the platinized ZrO₂/SiO₂/Al₂O₃ with a conversion maximum at 150 °C). As a consequence, for the Al-containing support, a *volcano*-shaped NO conversion curve in the temperature range between 75 and 300 °C in H₂-SCR-DeNO_x was observed, which could be based on a continuously coupled or overlaying mechanism of NO reduction by hydrogen and ammonia. In the case of Pt/ZrO₂/SiO₂, the NH₃-SCR-DeNO_x-based NO reduction started intensely above 150 °C, resulting in a split conversion curve with two maxima. Thus, the formed NH₃ reduced NO_x above 150 °C and thus explained the increase in the NO conversion during the H₂-SCR-DeNO_x process. Based on this result, it could be further hypothesized that, in the temperature range between 150 and 250 °C, the H₂-SCR-DeNO_x reaction is dominated through the NH₃-SCR-DeNO_x process (Equations (6) and

Catalysts 2025, 15, 483 7 of 16

(7)). The in situ NH₃ formed at lower temperatures, as confirmed by in situ DRIFTS measurements (via Equation (8), Figure S8, Table S4), was temporarily stored at the acid sites of the support and desorbed in this temperature range (e.g., [5,29,30]):

$$4 \text{ NO} + 4 \text{ NH}_3 + \text{O}_2 \rightarrow 4 \text{ N}_2 + 6 \text{ H}_2\text{O}$$
 (6)

$$4 \text{ NO} + 4 \text{ NH}_3 + 3 \text{ O}_2 \rightarrow 4 \text{ N}_2\text{O} + 6 \text{ H}_2\text{O}$$
 (7)

$$2 \text{ NO} + 5 \text{ H}_2 \rightarrow 2 \text{ NH}_3 + 2 \text{ H}_2\text{O}$$
 (8)

To further prove if NH₃-SCR-DeNO_x dominated above 150 °C over Pt-containing catalysts, we performed NH₃-assisted H₂-SCR-DeNO_x over both Pt/ZrO₂/SiO₂ and Pt/ZrO₂/SiO₂/Al₂O₃ (Figures S9 and S10). It can be seen that the NH₃-SCR-DeNO_x process started at lower temperatures over Pt/ZrO₂/SiO₂/Al₂O₃ than for Pt/ZrO₂/SiO₂. This was further supported for H₂-SCR-DeNO_x with pre-adsorbed NH₃ (Figure S11) over Pt/ZrO₂/SiO₂ and Pt/ZrO₂/SiO₂/Al₂O₃. Again, it was shown that N₂O preferentially formed as a result of the dissociative adsorption of NO below 200 °C over Pt/ZrO₂/SiO₂.

Above 250 °C, NO oxidation to NO₂ takes place (Equation (9)), resulting in a continuous decrease in the NO concentration in the reaction gas:

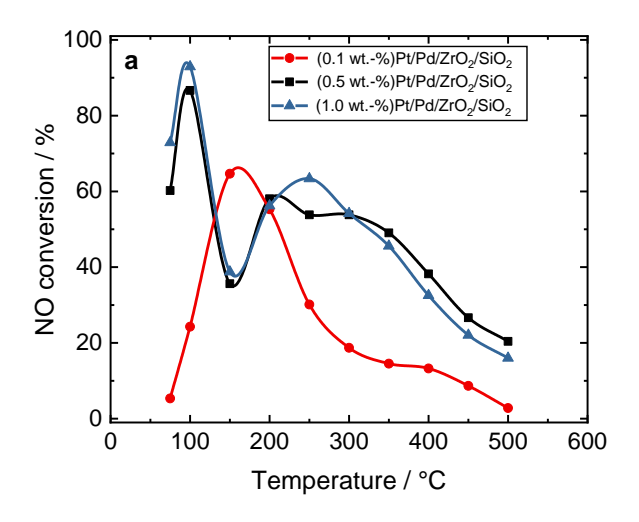
$$2 \text{ NO} + \text{O}_2 \rightarrow 2 \text{ NO}_2 \tag{9}$$

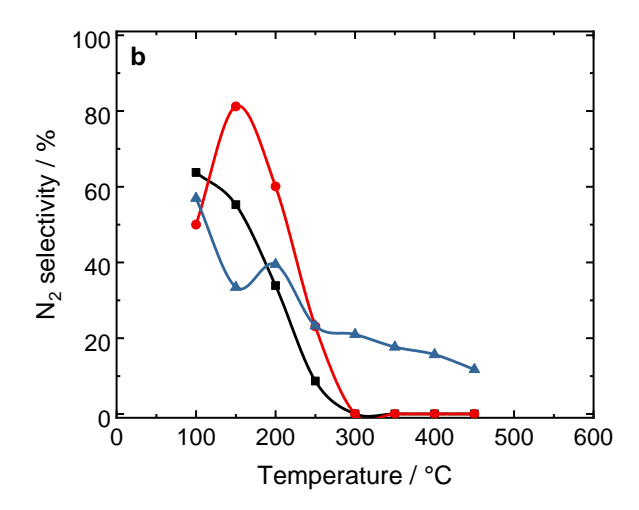
To clarify the role of each applied noble metal, in addition to H₂-SCR-DeNO_x, we performed NH₃-SCR-DeNO_x (Figure S11) over the Pd-containing counterparts. A comparison of H₂-SCR-DeNO_x over Pt- and Pd-containing catalysts (Figures 1 and S6) revealed that NO conversion occurred over both samples. In contrast, for NH₃-SCR-DeNO_x over both catalysts (Figure S12), the NO conversion occurred over Pt-containing catalysts, while NH₃ was oxidized mainly to NO over Pd-containing materials.

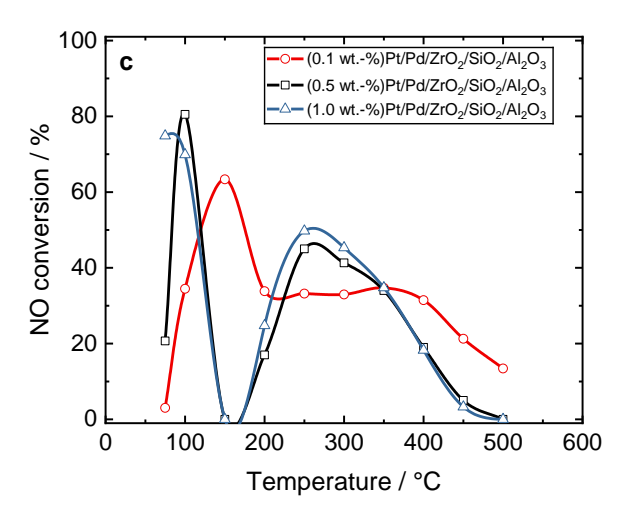
2.1.3. Effect of Precious Metal Loading

Figure S13 compares the NO conversion and N₂ selectivity over the Pt- and Pt/Pd-containing catalysts during H₂-SCR-DeNO_x. Among the evaluated samples, the Pt/Pd combinations supported on ZrO₂/SiO₂ had the highest N₂ selectivity. Thus, we then focused on the loading of precious metals over both ZrO₂/SiO₂- and ZrO₂/SiO₂/Al₂O₃-supported materials. Figure 3 reveals the activity and N₂ selectivity of the Pt/Pd-containing ZrO₂/SiO₂ and ZrO₂/SiO₂/Al₂O₃ plotted versus temperature with various noble metal concentrations (0.1–1.0 wt.-%) in H₂-SCR-DeNO_x. Among the ZrO₂/SiO₂-based catalysts, the NO conversion above 80% below 150 °C was achieved over (1.0 wt.-%)Pt/Pd/ZrO₂/SiO₂. Otherwise, the N₂ selectivity over this sample was below 60% up to 200 °C. For the samples with loadings of 0.5–1.0 wt.-% supported on ZrO₂/SiO₂/Al₂O₃, no NO conversion at 150 °C was detected. This significant drop in activity appeared as H₂ was completely consumed at 150 °C, while any NO was adsorbed over this type of support. Above 150 °C, NO oxidation started to dominate over the Pt/Pd/ZrO₂/SiO₂/Al₂O₃ catalyst.

Catalysts 2025, 15, 483 8 of 16







Catalysts 2025, 15, 483 9 of 16

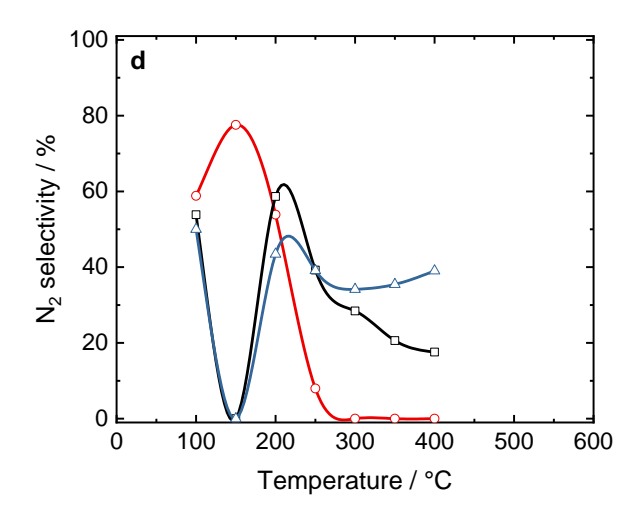


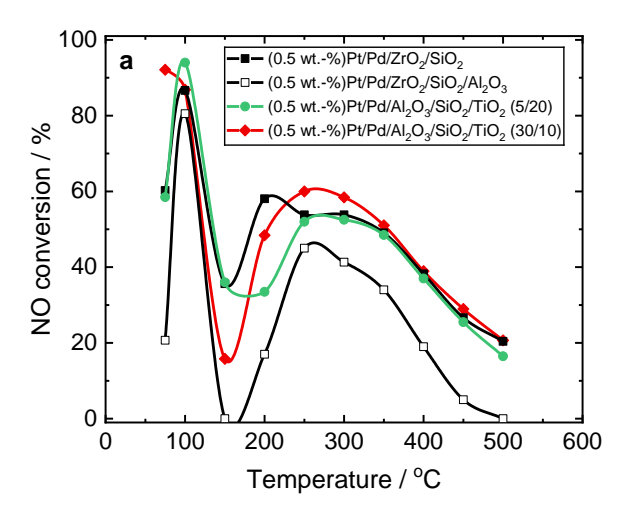
Figure 3. (**a**,**c**) NO conversion and (**b**,**d**) N₂ selectivity over Pt/Pd-containing ZrO₂/SiO₂ and ZrO₂/SiO₂/Al₂O₃ catalysts during H₂-SCR-DeNO_x; (**a**,**b**) and (**c**,**d**) sample labels are equal; reaction conditions: $m_K = 0.1$ g, c(NO) = 200 ppm, $c(H_2) = 2000$ ppm, $c(O_2) = 10$ vol.-%, diluted in He, F_{TOT} = 200 mL min⁻¹, GHSV = 30,000 h⁻¹.

As the loading of the noble metals reduced, the maximum NO reduction shifted progressively to higher temperatures. The catalyst with the lowest Pt/Pd loading of 0.1 wt.-% showed a more pronounced *volcano*-shaped conversion between 100 and 300 °C. The lower NO conversion of the material with 0.1 wt.-% loading and the enhanced N2 selectivity at 150 °C (ca. 80%) indicated the lower accessibility of the precious metal species to reactant molecules. Also, this material resulted in the higher oxidation of NO to NO2, which was reflected by the drop in the N2 selectivity above 300 °C. A similar trend was observed in the case of the samples based on the ZrO2/SiO2/Al2O3 support. Among the investigated series of Pt/Pd-containing samples, the (0.5 wt.-%)Pt/Pd/ZrO2/SiO2 catalysts had the optimum activity and N2 selectivity during H2-SCR-DeNOx (i.e., below 150 °C). In addition, similar conversion and selectivity were found for the Pt- and Pt-Pd-containing oxides (with the exception of Pt/ZrO2/SiO2) in NH3-SCR-DeNOx (Figure S10), indicating that both reactions proceeded over the same precious metal species.

2.1.4. Effect of Support Composition

Figure 4 compares the activity and N_2 selectivity of the (0.5 wt.-%) Pt/Pd-loaded ZrO₂/SiO₂, ZrO₂/SiO₂/Al₂O₃, and commercial titania-containing Al₂O₃/SiO₂/TiO₂ (5/20, 30/10) in H₂-SCR-DeNO_x. A maximum NO conversion of 94% at 100 °C was obtained with Al₂O₃/SiO₂/TiO₂ (5/20), followed by both Al₂O₃/SiO₂/TiO₂ (30/10; i.e., with a higher silica amount) and ZrO₂/SiO₂/Al₂O₃ (88%). It was remarkable that the maximum NO conversion was obtained at 100 °C for all silica-based catalysts. Also, a *volcano*-type behavior in NO conversion was observed for all catalysts. Still, (0.5 wt.-%)Pt/Pd/ZrO₂/SiO₂ showed the highest selectivity toward N₂ (80% at 100 °C) among the investigated materials (with N₂ selectivity below 60% at this temperature).

Catalysts 2025, 15, 483 10 of 16



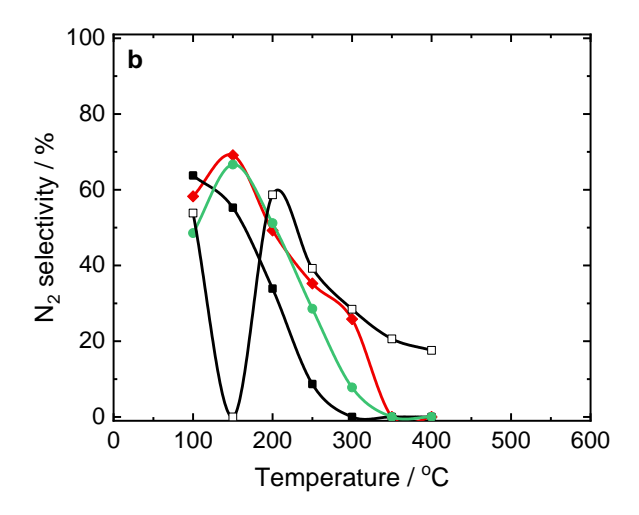


Figure 4. (a) NO conversion and (b) N₂ selectivity over Pt/Pd-containing ZrO₂/SiO₂, ZrO₂/SiO₂/Al₂O₃, Al₂O₃/SiO₂/TiO₂ (5/20 and 30/10) catalysts during H₂-SCR-DeNO_x; (a,b) sample labels are equal; reaction conditions: $m_K = 0.1$ g, c(NO) = 200 ppm, $c(H_2) = 2000$ ppm, $c(O_2) = 10$ vol.-%, diluted in He, F_{TOT} = 200 mL min⁻¹, GHSV = 30,000 h⁻¹.

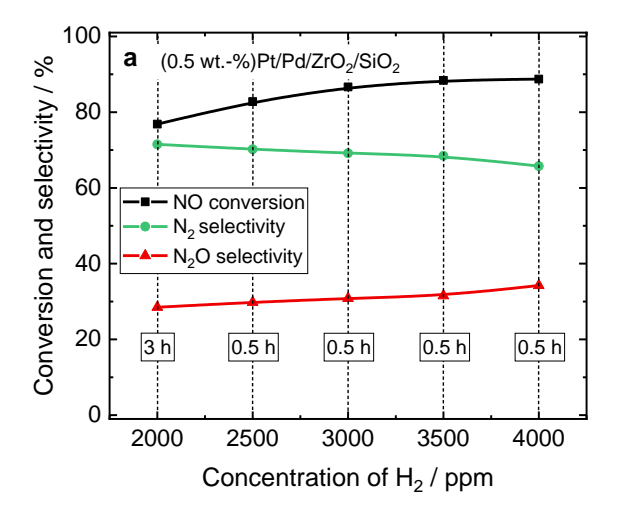
Additionally, the (0.5 wt.-%)Pt/Pd/ZrO₂/SiO₂ catalyst was tested in six consecutive cycling tests with heating to 500 °C and cooling down to 30 °C (Figure S14) as well as in the 24 h steady-state at 100 °C for 24 h (Figure S15). This catalyst showed stable NO conversion and selectivity during the applied temperature and time. In the following studies, this material will be coated on monolith and investigated as a catalyst applied in H_2 engines in the feed gas (containing above 12 wt.-% H_2 O).

The morphological images of the catalyst before and after the reactions are provided to illustrate the stability of the catalyst. Figure S16 shows the ToF-SIMS images collected from the surface of (0.5 wt.-%)Pt/Pd/ZrO₂/SiO₂ for the fresh sample, after H₂-SCR-DeNO_x for 24 h at 100 °C, and after six cycles during H₂-SCR-DeNO_x. The obtained results showed that the distribution of Pd⁺ and Pt⁺ ions on the surface of the tested materials was homogeneous and did not change in the case of samples tested after the reaction. Table S5 presents the intensity ratios of selected ions calculated from the collected spectra. Among all investigated samples, minor changes appeared in the signal coming from the Pd⁺ and Pt⁺ ions with respect to the main carrier components (Si⁺ and Zr⁺ ions).

Catalysts 2025, 15, 483 11 of 16

2.1.5. Effect of Hydrogen Concentration

Figure 5 shows the NO conversion as well as the N₂ and N₂O selectivity of (0.5 wt.-%) Pt/Pd-containing ZrO₂/SiO₂ and ZrO₂/SiO₂/Al₂O₃ in H₂-SCR-DeNO_x at 120 °C with varied H₂ concentrations at 120 °C. After 3 h of conditioning in the feed containing 2000 ppm of hydrogen, the its concentration of the catalysts was increased up to 4000 ppm (in intervals of 0.5 h), while keeping the total flow content. For the ZrO₂/SiO₂-based catalyst, an increase in NO conversion from 77 to 89% was observed with increasing the H₂ concentration to 4000 ppm. However, the enhanced NO conversion was accompanied by the N₂ selectivity dropping from 71 to 66%. Thus, the N₂O selectivity of Pt/Pd/ZrO₂/SiO₂ increased with increasing H₂ concentration in the feed at 120 °C. Hence, the accumulation of NO over time at the surface of the ZrO₂/SiO₂-based catalyst led to the formation of N₂O (Equation (2)). Conversely, for the ZrO₂/SiO₂-based catalyst, an increase in NO conversion of 21% was observed, resulting in an increase in N₂ selectivity from 44 to 55%, indicating different reaction pathways over the second catalyst (i.e., according to the NO reduction with H₂, Equation (1); Figures S17 and S18). A schematic representation of the above-described mechanism is presented in Figure 6.



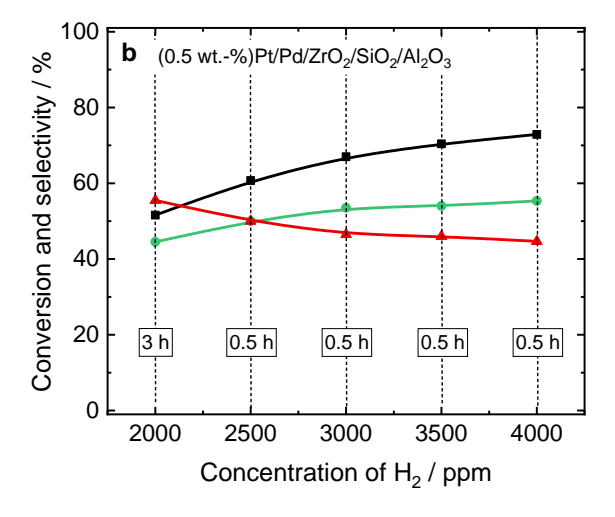


Figure 5. NO conversion and N₂ selectivity over (a) Pt/Pd-containing ZrO₂/SiO₂ and (b) ZrO₂/SiO₂/Al₂O₃ during H₂-SCR-DeNO_x with various H₂ concentrations at 120 °C; (a,b) labels are equal; reaction conditions: $m_K = 0.1$ g, c(NO) = 200 ppm, $c(H_2) = 2000$ –4000 ppm, $c(O_2) = 10$ vol.-%, diluted in He, F_{TOT} = 200 mL min⁻¹, GHSV = 30,000 h⁻¹.

Catalysts 2025, 15, 483 12 of 16

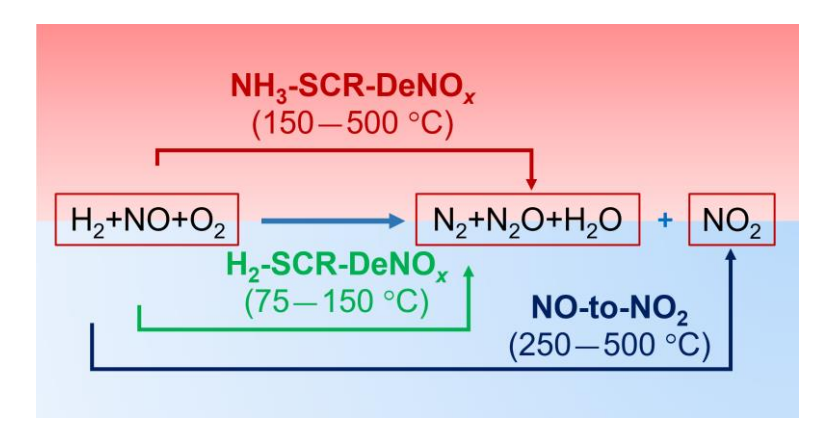


Figure 6. Schematic representation of the reaction mechanism.

3. Catalyst Preparation and Characterization

Commercially available silica-containing supports such as ZrO₂/SiO₂ (Luxfer Mel Technologies, Manchester, UK; XCO 2699; 10 wt.-% SiO₂), ZrO₂/SiO₂/Al₂O₃ (Sasol Germany GmbH, Hamburg Germany; Siralox SZ 25/15; 25 wt.-% SiO₂, 15 wt.-% ZrO₂), Al₂O₃/SiO₂/TiO₂ (5/20) (Sasol Germany GmbH, Hamburg, Germany; Siralox 5/Ti 20; 5 wt.-% SiO₂, 20 wt.-% TiO₂), and Al₂O₃/SiO₂/TiO₂ (30/10) (Sasol Germany GmbH, Hamburg, Germany; Siralox 30/Ti 10; 30 wt.-% SiO₂, 10 wt.-% TiO₂) were used in this study. These supports were impregnated by the incipient wetness impregnation (IWI) method with Pt, Pd, and Pt/Pd precursors. The total precious metal contents of the resulting catalyst were adjusted to 0.1, 0.5, and 1 wt.-%. Therefore, appropriate amounts of aqueous solutions of (NH₃)₄Pt(NO₃)₂ (99 wt.-%, Fisher Scientific GmbH, Schwerte, (NH₃)₄Pd(NO₃)₂ (99 wt.-%, Stanford Advanced Materials, Lake Forest, CA, USA) or their mixtures (based on H₂O absorption analysis in advance) were mixed with the supports. Bimetallic Pt/Pd samples were prepared with a ratio of n(Pt)/n(Pd) = 1.0. The resulting wet powders were dried at 120 °C and afterwards calcined at 550 °C (1 h, 3 °C min-1). The sample abbreviations include information about the intended loading of the noble metal and selected support, e.g., (0.5 wt.-%)Pt/ZrO₂/SiO₂.

The information regarding the physico-chemical characterization of the selected samples, including XRD, N_2 sorption, inductively coupled plasma–optical emission spectroscopy (ICP-OES), temperature-programmed desorption of ammonia (NH₃-TPD), time-of-flight secondary ion mass spectrometry (ToF-SIMS), and in situ DRIFTS, can be found in the Supplementary Information.

4. Catalytic Studies

The catalytic experiments were carried out with 0.1 g of catalyst, with a particle size fraction of 200–400 µm, placed in a fixed-bed quartz tube reactor (ID: 6 mm, L: 200 mm). Before each experiment, the catalyst was activated at 350 °C for 1.5 h at a flow rate of 50 mL min⁻¹ of pure helium (He). The reactor was then cooled to 50 °C. The total gas phase flow was 200 mL min⁻¹, corresponding to a gas hourly space velocity (GHSV) of 30,000 h⁻¹. The feed consisting of c(NO) = 200 ppm, $c(H_2) = 2000$ ppm, and $c(O_2) = 10$ vol.-% was diluted in He. Our target application of H₂-SCR-DeNO_x in the H₂-fired internal combustion engines for combined heat and power (CHP) with exhaust gas temperatures below 150 °C did not require catalytic experiments with NO₂ in the feed gas. The reaction was carried out at atmospheric pressure up to 500 °C in increments of 25–50 °C. At each temperature, the reaction was allowed to stabilize for 45 min before quantitative analysis of the product gas composition, and the resulting concentration was obtained. The reagents and products were analyzed continuously using a QMS MKS Cirrus-3 (Munich, Germany) connected directly to the reactor outlet via a heated capillary.

Catalysts 2025, 15, 483 13 of 16

The NO conversion (X(NO)) was determined using the formula $X(NO) = ([c(NO)_{int} c(NO)_{int} c(NO)_{int})/c(NO)_{int}) \times 100\%$. In this equation, $c(NO)_{int}$ and $c(NO)_{out}$ represent the NO concentration in the inlet and outlet gas, respectively. To maintain the accuracy of the measurements, the He line signal was used as an internal standard to compensate for small variations in operating pressure. During the H₂-SCR-DeNO_x reaction, in addition to N₂, N₂O and NO_x were identified. To calculate the selectivity toward N₂ formation, the equation $S(N_2) = (c(N_2))/(c(N_2) + c(N_2O) + 0.5c(NO_2)) \times 100\%$ was applied. In this expression, $c(N_2)$, $c(N_2O)$, and $c(NO_2)$ correspond to the concentrations of N₂, N₂O, and NO₂ in the flue gases, respectively. The experimental uncertainty in the calculated NO conversion was found to be ±5% (as indicated by repeated measurements of identical catalysts).

For the stop-flow experiments, the reaction was carried out for 45 min at 100 or 150 °C with the feed gas as specified above. After that time, the feed was exchanged with a flow of pure helium (50 mL min⁻¹). After 90 min of purging, the temperature was increased up to 500 °C with a heating step of 10 °C min⁻¹.

Selected samples were investigated for the selective catalytic reduction of NO_x with ammonia (NH₃-SCR-DeNO_x) and combined H₂-NH₃-SCR-DeNO_x, following the same procedure as applied for H₂-SCR-DeNO_x. The total gas phase flow was 200 mL min⁻¹ (120 mL min⁻¹ for NH₃-SCR-DeNO_x), consisting of c(NO) = 200 ppm, c(H₂) = 2000 ppm, c(NH₃) = 1000 ppm, c(O₂) = 10 vol.-% diluted in helium (c(NO) = 1000 ppm, c(NH₃) = 1000 ppm, and c(O₂) = 10 vol.-% diluted in helium). The gas hourly space velocity (GHSV) was also set at 30,000 h⁻¹. Again, the experimental uncertainty of the calculated NO conversion was found to be ±5% (as indicated by repeated measurements of identical catalysts).

5. Conclusions

Pt- and/or Pd-deposited on the different silica supports were investigated in H2-SCR-DeNO_x under lean reaction conditions with 10 vol.-% O₂. The Pt-Pd-containing catalysts reported for the first time in this paper outperformed monometallic catalysts. Different catalyst compositions had the highest activity and N₂ selectivity below 150 °C for Pt/Pd/ZrO₂/SiO₂, with a total noble metal loading of 0.5 wt.-%. This catalyst showed high stability during time-on-stream H2-SCR-DeNO_x. H2 was completely consumed at 150 °C during H2-SCR-DeNO_x over the applied catalysts. In addition to H2-SCR-DeNO_x, selected materials were examined in NH₃-SCR-DeNO_x as well as NH₃-assisted H2-SCR-DeNO_x. A comparison of the catalytic results from H2-SCR-DeNO_x, (H2-)NH₃-SCR-DeNO_x, and stop-flow H2-SCR-DeNO_x indicated that in the temperature range between 150 and 250 °C, a continuously coupled or overlaying mechanism of NO reduction by hydrogen and ammonia based on NH₃ formation at lower temperatures, which was temporarily stored at acid sites of the support and desorbed in this temperature range, could be postulated. The oxidation of NO appeared above 250 °C.

Supplementary Materials: The following supporting information can be downloaded at: https://www.mdpi.com/article/10.3390/catal15050483/s1, Figure S1: XRD patterns of Pt- and Pd-containing catalysts; * - ZrO₂ (cubic), + - TiO₂ (anatase); Figure S2: (a,b) N₂ sorption isotherms collected at -196 °C and (c,d) BJH pore width distribution of Pt- and Pd-containing catalysts; (a,c) and (b,d) sample labels are identical. Figure S3: NH₃-TPD profiles of Pt-, Pd- and Pt/Pd-containing catalysts: (a) ZrO₂/SiO₂, (b) ZrO₂/SiO₂/Al₂O₃, and (c) Al₂O₃/SiO₂/TiO₂. Table S1: The elemental analysis results of Pt- and/or Pd-containing catalysts (ω: mass fractions; ω(TOT): total mass fractions of noble metals). Table S2: The textural properties of Pt- and/or Pd-containing catalysts: specific surface area (A_{S(BET)}), micropore pore volume (VMIC), mesopore pore volume (VMES), and total pore volume (VTOT). Table S3: The results of NH₃-TPD of Pt- and/or Pd-containing catalysts: concentration of acid sites (CNH₃) and acid site density (ANH₃). Figure S4: Examples of raw data, showing the

Catalysts 2025, 15, 483 14 of 16

temperature-dependent disappearance of H_2 (m/z = 2) from the reaction mixture due to its oxidation (m/z, mass-to-charge ratio; 1 scan = 19 s). Figure S5: Raw data for H₂-SCR-DeNO_x over pure (a) ZrO₂/SiO₂ and (b) ZrO₂/SiO₂/Al₂O₃ supports (without metals); (a,b) labels are equal; reaction conditions: $m_K = 0.1 \text{ g}$, c(NO) = 200 ppm, $c(H_2) = 2000 \text{ ppm}$, $c(O_2) = 10 \text{ vol.-}\%$, diluted in He, $F_{TOT} = 0.00 \text{ ppm}$ 200 mL min⁻¹, GHSV = 30,000 h⁻¹ (m/z, mass-to-charge ratio; 1 scan = 19 s). H₂ (m/z 2), NH₃ (m/z 17) H₂O (m/z 18), N₂ (m/z 28), NO (m/z 30), N₂O (m/z 44), and NO₂ (m/z 46). Figure S6: Raw data for H₂-SCR-DeNO_x over (a,b) Pt-containing ZrO₂/SiO₂ and ZrO₂/SiO₂/Al₂O₃ catalysts, and (c,d) Pdcontaining ZrO₂/SiO₂ and ZrO₂/SiO₂/Al₂O₃ catalysts; (a–d) labels are equal; Reaction conditions: mk = 0.1 g, c(NO) = 200 ppm, $c(H_2)$ = 2000 ppm, $c(O_2)$ = 10 vol.-%, diluted in He, F_{TOT} = 200 mL min⁻¹, GHSV = $30,000 \text{ h}^{-1}$ (m/z, mass-to-charge ratio; 1 scan = 19 s). H₂ (m/z 2), N₂ (m/z 28), NO (m/z 30), N₂O (m/z 44), and NO₂ (m/z 46). Figure S7: (a) NO conversion and (b) selectivity over Pt-containing ZrO₂/SiO₂ and ZrO₂/SiO₂/Al₂O₃ catalysts during NH₃-SCR-DeNO_x; (a) and (b) sample labels are equal; reaction conditions: $m\kappa = 0.1$ g, c(NO) = 1000 ppm, $c(NH_3) = 1000$ ppm, $c(O_2) = 10$ vol.-%, diluted in He, Ftot = 120 mL min⁻¹, GHSV = 30,000 h⁻¹. Figure S8: DRIFT spectra of the (a,c) Ptcontaining ZrO₂/SiO₂ and (b,d) ZrO₂/SiO₂/Al₂O₃ catalysts during H₂-SCR-DeNO_x. Table S4: Assignment of the identified peaks [31,32]. Figure S9: Raw data for H₂-NH₃-SCR-DeNO_x over (a) Ptcontaining ZrO₂/SiO₂ and (b) ZrO₂/SiO₂/Al₂O₃ catalysts; (a–c) labels are equal; Reaction conditions: $m_K = 0.1 \text{ g}$, c(NO) = 200 ppm, $c(H_2) = 2000 \text{ ppm}$, $c(NH_3) = 1000 \text{ ppm}$, $c(O_2) = 10 \text{ vol.-}\%$, diluted in He, $F_{TOT} = 200 \text{ mL min}^{-1}$, $GHSV = 30,000 \text{ h}^{-1}$ (m/z, mass-to-charge ratio; 1 scan = 19 s). H_2 (m/z 2), NH_3 (m/z17), H₂O (m/z 18), N₂ (m/z 28), NO (m/z 30), N₂O (m/z 44), and NO₂ (m/z 46). Figure S10: Comparison of the (a,c) NO conversion and (b,d) N2 selectivity during H2-SCR-, NH3-SCR- and H2-NH3-SCR-DeNO_x over Pt-containing ZrO₂/SiO₂ and ZrO₂/SiO₂/Al₂O₃ catalysts. Reaction conditions for H₂-NH₃-SCR-DeNO_x: $m_K = 0.1$ g, c(NO) = 200 ppm, $c(H_2) = 2000$ ppm, $c(NH_3) = 1000$ ppm, $c(O_2) = 10$ vol.-%, diluted in He, Ftot= 200 mL min⁻¹, GHSV = 30,000 h⁻¹. Figure S11: Temperature-programmed desorption over (a) Pt-containing ZrO₂/SiO₂ and (b) ZrO₂/SiO₂/Al₂O₃ catalysts: NH₃ desorption in NO+O₂+H₂; Reaction conditions: $m_K = 0.1$ g, adsorption: $c(NH_3) = 3000$ ppm, diluted in He, 45 min, 50 mL min⁻¹, desorption: pure He, 90 min, 50 mL min⁻¹, surface reaction: c(NO) = 3000 ppm, $c(H_2) =$ 1000 ppm and $c(O_2) = 10$ vol.-%, diluted in He, 50 mL min⁻¹; (m/z, mass-to-charge ratio; 1 scan = 19 s). NH₃ (m/z 17), H₂O (m/z 18), N₂ (m/z 28), NO (m/z 30), N₂O (m/z 44), NO₂ (m/z 46), and H₂ (m/z 2). Figure S12: Raw data for NH₃-SCR-DeNO_x over (a,b) Pt-containing ZrO₂/SiO₂ and ZrO₂/SiO₂/Al₂O₃ catalysts, and (c,d) Pd-containing ZrO₂/SiO₂ and ZrO₂/SiO₂/Al₂O₃ catalysts; (a–d) labels are equal; Reaction conditions: $m_K = 0.1$ g, c(NO) = 1000 ppm, $c(NH_3) = 1000$ ppm, $c(O_2) = 10$ vol.-%, diluted in He, $F_{TOT} = 120 \text{ mL min}^{-1}$, $GHSV = 30,000 \text{ h}^{-1}$ (m/z, mass-to-charge ratio; 1 scan = 19 s). NH₃ (m/z 17), H₂O (m/z 18), N₂ (m/z 28), NO (m/z 30), N₂O (m/z 44), and NO₂ (m/z 46). Figure S13: (a) NO conversion and (b) N2 selectivity over Pt- and Pt/Pd-containing ZrO2/SiO2 and ZrO2/SiO2/Al2O3 catalysts during H₂-SCR-DeNO_x; (a,b) sample labels are equal; reaction conditions: $m\kappa = 0.1$ g, c(NO) = 200 ppm, $c(H_2)$ = 2000 ppm, $c(O_2)$ = 10 vol.-%, diluted in He, F_{TOT} = 200 mL min⁻¹, GHSV = 30,000 h⁻¹. Figure S14: Comparison of the (a) activity and (b) selectivity of (0.5 wt.-%)Pt/Pd/ZrO₂/SiO₂ during heating (30-500 °C) and cooling down (500–30 °C) during H₂-SCR-DeNO_x. Reaction conditions: mκ = 0.1 g, c(NO) = 200 ppm, $c(H_2)$ = 2000 ppm, $c(O_2)$ = 10 vol.-%, diluted in He, F_{TOT} = 200 mL min⁻¹, GHSV = 30,000 h^{-1} , linear heating rate of 10 °C min⁻¹ (m/z, mass-to-charge ratio; 1 scan = 19 s). NO (m/z 30), N₂ (m/z 28), N₂O (m/z 44), and H₂ (m/z 2). Figure S15: Long-term experiments over (0.5 wt.-%)Pt/Pd/ZrO₂/SiO₂ during H₂-SCR-DeNO_x at 100 °C for 24 h; reaction conditions: $m_K = 0.1$ g, $c(NO) = 200 \text{ ppm}, c(H_2) = 2000 \text{ ppm}, c(O_2) = 10 \text{ vol.-}\%, \text{ diluted in He, Ftot} = 200 \text{ mL min}^{-1}, \text{GHSV} = 200 \text{ mL min}^{-1}$ $30,000 \text{ h}^{-1}$ (m/z, mass-to-charge ratio; 1 scan = 19 s). H_2 (m/z 2), H_2 O (m/z 18), N_2 (m/z 28), N_3 O (m/z 30), N₂O (m/z 44), and NO₂ (m/z 46). Figure S16: ToF-SIMS images collected from the surface of (0.5 wt.-%)Pt/Pd/ZrO₂/SiO₂ (tc, total counts), (a) fresh sample, (b) after H₂-SCR-DeNO_x for 24 h at 100 °C, (c) after H₂-SCR-DeNO_x with H₂O, and (d) after six cycles during H₂-SCR-DeNO_x. Table S5: Intensity ratios of selected ions calculated based on ToF-SIMS spectra collected from the surface of the samples. Figure S17: Comparison of the (a,b) NO conversion and N2 selectivity during (c) H2-SCR-DeNOx and (d) NH3-SCR-DeNOx over (a,c) Pt-containing and (b,d) Pt/Pd-containing ZrO2/SiO2 and

Catalysts 2025, 15, 483 15 of 16

 $ZrO_2/SiO_2/Al_2O_3$ catalysts; (a,b) and (c,d) sample labels are equal. Figure S18: (a) NO conversion and (b–d) selectivity over Pt- and Pt/Pd-containing ZrO_2/SiO_2 and $ZrO_2/SiO_2/Al_2O_3$ catalysts during NH₃-SCR-DeNO_x; a-d) sample labels are equal; reaction conditions: $m_K = 0.1$ g, c(NO) = 1000 ppm, $c(NH_3) = 1000$ ppm, $c(O_2) = 10$ vol.-%, diluted in He, $F_{TOT} = 120$ mL min⁻¹, GHSV = 30,000 h⁻¹.

Author Contributions: M.J.: conceptualization, methodology, investigation, data curation, writing—original draft, writing—review and editing, supervision, project management. A.O.H.: investigation, data curation, writing—original draft. J.D.: conceptualization, methodology, investigation, writing—review and editing. J.G.: investigation, data curation. A.G.: investigation, data curation. U.S.: review. R.G.: review. All authors have read and agreed to the published version of the manuscript.

Funding: M.J. acknowledges a DFG Research Grant JA 2998/2-1. M.J., J.D., and R.G. acknowledge Bundesministerium für Wirtschaft und Klimaschutz Project FDZ 03EE5122B.

Data Availability Statement: Data are contained within this article and Supplementary Materials.

Conflicts of Interest: The authors do not have any conflicts of interest.

References

- 1. Skowron, A.; Lee, D.S.; De León, R.R. Variation of radiative forcings and global warming potentials from regional aviation NO_x emissions. *Atmos. Environ.* **2015**, *104*, 69–78.
- 2. Hui, K.; Yuan, Y.; Xi, B.; Tan, W. A review of the factors affecting the emission of the ozone chemical precursors VOCs and NO_x from the soil. *Environ. Int.* **2023**, *172*, 107799.
- 3. Zhao, X.; Zhang, X.; Xu, Y.; Liu, Y.; Wang, X.; Yu, Q. The effect of H₂O on the H₂-SCR of NO_x over Pt/HZSM-5. *J. Mol. Catal. A Chem.* **2015**, 400, 147–153.
- 4. Cao, L.; Wang, Q.; Yang, J. Ultrafine Pt particles directed by polyvinylpyrrolidone on zeolite beta as an efficient low-temperature H2-SCR catalyst. *J. Environ. Chem. Eng.* **2020**, *8*, 103631.
- 5. Hu, Z.; Yang, R.T. 110th Anniversary: Recent progress and future challenges in selective catalytic reduction of NO by H₂ in the presence of O₂. *Ind. Eng. Chem. Res.* **2019**, *58*, 10140–10153.
- 6. Liu, Y.; Tursun, M.; Yu, H.; Wang, X. Surface property and activity of Pt/Nb₂O₅-ZrO₂ for selective catalytic reduction of NO by H₂. *Mol. Catal.* **2019**, 464, 22–28.
- 7. Choi, M.; Yook, S.; Kim, H. Hydrogen spillover in encapsulated metal catalysts: New opportunities for designing advanced hydroprocessing catalysts. *ChemCatChem* **2015**, *7*, 1048–1057.
- 8. Hong, Z.; Sun, X.; Wang, Z.; Zhao, G.; Li, X.; Zhu, Z. Pt/SSZ-13 as an efficient catalyst for the selective catalytic reduction of NO_x with H₂. Catal. Sci. Technol. **2019**, *9*, 3994–4001.
- 9. Li, L.; Wu, P.; Yu, Q.; Wu, G.; Guan, N. Low temperature H₂-SCR over platinum catalysts supported on Ti-containing MCM-41. *Appl. Catal. B Environ.* **2010**, 94, 254–262.
- 10. Zhang, Y.; Xu, S.; Li, J.; He, E.; Liu, Z. Unraveling the promotional effect of Co on the Pd/TiO₂ Catalyst for H₂-SCR of NO_x in the presence of oxygen. *J. Phys. Chem. C* **2023**, 127, 7248–7256.
- 11. Park, D.C.; Moon, S.; Song, J.H.; Kim, H.; Lee, E.; Lim, Y.H.; Kim, D.H. Widening the operating window of Pt/ZSM-5 catalysts for efficient NO_x removal in H₂-SCR: Insights from thermal aging. *Catal. Today* **2024**, 425, 114318.
- 12. Schott, F.J.P.; Balle, P.; Adler, J.; Kureti, S. Reduction of NO_x by H₂ on Pt/WO₃/ZrO₂ catalysts in oxygen-rich exhaust. *Appl. Catal. B Environ.* **2009**, *87*, 18–29.
- 13. Yu, Q.; Richter, M.; Li, L.; Kong, F.; Wu, G.; Guan, N. The promotional effect of Cr on catalytic activity of Pt/ZSM-35 for H₂-SCR in excess oxygen. *Catal. Commun.* **2010**, *11*, 955–959.
- 14. Hamada, S.; Hibarino, S.; Ikeue, K.; Machida, M. Preparation of supported Pt-M catalysts (M = Mo and W) from anion-exchanged hydrotalcites and their catalytic activity for low temperature NO-H₂-O₂ reaction. *Appl. Catal. B Environ.* **2007**, 74, 197–202.
- 15. Liu, Z.; Li, J.; Woo, S.I. Recent advances in the selective catalytic reduction of NO x by hydrogen in the presence of oxygen. *Energy Environ. Sci.* **2012**, *5*, 8799–8814.
- 16. Shibata, J.; Hashimoto, M.; Shimizu, K.; Yoshida, H.; Hattori, T.; Satsuma, A. Factors controlling activity and selectivity for SCR of NO by hydrogen over supported platinum catalysts. *J. Phys. Chem. B* **2004**, *108*, 18327–18335.

Catalysts 2025, 15, 483 16 of 16

17. Costa, C.N.; Efstathiou, A.M. Low-temperature H₂-SCR of NO on a novel Pt/MgO-CeO₂ catalyst. *Appl. Catal. B Environ.* **2007**, 72, 240–252.

- 18. Yu, Q.; Richter, M.; Kong, F.; Li, L.; Wu, G.; Guan, N. Selective catalytic reduction of NO by hydrogen over Pt/ZSM-35. *Catal. Today* **2010**, *158*, 452–458.
- 19. Duan, K.; Chen, B.; Zhu, T.; Liu, Z. Mn promoted Pd/TiO₂-Al₂O₃ catalyst for the selective catalytic reduction of NO_x by H₂, *Appl. Catal. B Environ.* **2015**, *176*, 618–626.
- 20. Patel, V.K.; Sharma, S. Effect of oxide supports on palladium based catalysts for NO reduction by H₂-SCR. *Catal. Today* **2021**, 375, 591–600.
- 21. Moon, S.; Park, D.C.; Lee, E.; You, Y.-W.; Heo, I.; Kim, Y.J.; Kim, D.H. Excellent activity and selectivity of Pd/ZSM-5 catalyst in the selective catalytic reduction of NO_x by H₂. *Environ. Res.* **2023**, 227, 115707.
- 22. Jabłońska, M.; Osorio Hernández, A. Selective catalytic reduction of nitrogen oxides with hydrogen (H₂-SCR-DeNO_x) over platinum-based catalysts. *ChemCatChem* **2024**, *16*, e202400977. https://doi.org/10.1002/cctc.202400977.
- 23. Mangla, O.; Roy, S. Monoclinic zirconium oxide nanostructures having tunable band gap synthesized under extremely non-equilibrium plasma conditions. *Proceedings* **2019**, *3*, 10.
- 24. Tan, D.; Lin, G.; Liu, Y.; Teng, Y.; Zhuang, Y.; Zhu, B.; Zhao, Q.; Qiu, J. Synthesis of nanocrystalline cubic zirconia using femtosecond laser ablation. *J. Nanoparticle Res.* **2011**, *13*, 1183–1190.
- 25. Chaiyo, P.; Duangsing, B.; Thumthan, O.; Nutariya, J.; Pukird, S. Electrical and gas sensing properties of TiO₂/GO nanocomposites for CO₂ sensor application. *J. Phys. Conf. Ser.* **2017**, *901*, 012095.
- 26. Schröder, D.; Kureti, S. Low-temperature NO_x reduction by H₂ on Mo-promoted Pt/ZrO₂ catalysts in lean exhaust gases. *Top. Catal.* **2023**, *66*, 787–796.
- 27. Li, X.; Zhang, X.; Xu, Y.; Liu, Y.; Wang, X. Influence of support properties on H₂ selective catalytic reduction activities and N₂ selectivities of Pt catalysts. *Chin. J. Catal.* **2015**, *36*, 197–203.
- 28. Park, J.-H.; Cho, J.H.; Kim, Y.J.; Kim, E.S.; Han, H.S.; Shin, C.-H. Hydrothermal stability of Pd/ZrO₂ catalysts for high temperature methane combustion. *Appl. Catal. B Environ.* **2014**, *160*, 135–143.
- 29. Farhan, S.M.; Wang, P.; Chen, Z.; Yin, J. Innovative catalysts for the selective catalytic reduction of NO_x with H₂: A systematic review. *Fuel* **2024**, *355*, 129364.
- 30. Guan, Y.; Liu, Y.; Lv, Q.; Wang, B.; Che, D. Review on the selective catalytic reduction of NO_x with H₂ by using novel catalysts. *J. Environ. Chem. Eng.* **2021**, *9*, 106770.
- 31. Eldridge, T.J.; Borchers, M.; Lott, P.; Grunwaldt, J.D.; Doronkin, D.E. Elucidating the role of the state of Pd in the H₂-SCR of NO_x by operando XANES and DRIFTS. *Catal. Sci. Technol.* **2024**, *14*, 4198–4210.
- 32. Fan, J.; Ning, P.; Song, Z.; Liu, X.; Wang, L.; Wang, J.; Wang, H.; Long, K.; Zhang, Q. Mechanistic aspects of NH₃-SCR reaction over CeO₂/TiO₂-ZrO₂-SO₄²⁻ catalyst: In situ DRIFTS investigation. *Chem. Eng. J.* **2018**, 334, 855–863.

Disclaimer/Publisher's Note: The statements, opinions and data contained in all publications are solely those of the individual author(s) and contributor(s) and not of MDPI and/or the editor(s). MDPI and/or the editor(s) disclaim responsibility for any injury to people or property resulting from any ideas, methods, instructions or products referred to in the content.